Ceramics International 48 (2022) 9681–9691

Contents lists available at ScienceDirect

Ceramics International

journal homepage: www.elsevier.com/locate/ceramint

Three routes for the synthesis of the bioceramic powder of the CaO-MgO-SiO_2 system

Chieko Yamagata [a,*], Daniel Rezende Leme [a], Vanessa Galvão Rodrigues [a], Gabriel Trindade Eretides [a], Andrea Cecilia Dorion Rodas [b]

[a] Nuclear and Energy Research Institute, Instituto de Pesquisas Energéticas e Nucleares, CCTM (Centro de Ciência e Tecnologia de Materiais), São Paulo, Brazil
[b] Biomedical Engineering, Federal University of ABC, Santo Andre, Brazil

ARTICLE INFO

Keywords:
Bioceramic
CaO-MgO-SiO_2 system
Synthesis
Sol-gel
Coprecipitation
Characterization

ABSTRACT

We report three routes for the synthesis of CaO-MgO-SiO_2 (CMS) bioceramic powder using different Si sources and synthesis procedures. The ceramic powders were synthesized from Na_2SiO_3 waste solution by the sol-gel process combined with co-precipitation (synthesis route I and synthesis route II), and from TEOS (tetraethyl orthosilicate) by conventional sol-gel (synthesis route III). Ceramic powders of the CMS multiphase system were obtained, including diopside, wollastonite, akermanite, monticellite and merwinite, which are suitable for application as biomaterial. These powders were sintered at 1200 °C for 2 h to obtain the CMS ceramics. The ceramics mostly contained diopside and wollastonite crystalline phases. Those ceramics when submitted to cytotoxicity tests revealed to be non-cytotoxic, according to ISO10993-5:2009. The ceramics were tested for in vitro bioactivity while soaked in simulated body fluid (SBF) solution. After 14 days, the presence of hydroxyapatite particles on the surface of ceramics was confirmed by Fourier Transform Infrared (FTIR) spectroscopy and Scanning Electron Microscopy (SEM) micrographs. The surfaces were completely covered with hydroxyapatite, after 21 days. In summary, CaO-MgO-SiO_2 (CMS) ceramic powder derived from three routes of synthesis have potential application in the biomedical area. However, further in-vitro and in-vivo studies are needed.

1. Introduction

During the past few decades, extensive research efforts have been directed towards the synthesis of different bioceramics. The main use of these bioceramics is for bone and dental root implants. The chemical composition and physical characteristics of the material such as surface morphology and chemical resistance determine the cellular response to the ceramic from the surrounding tissue [1,2]. Bio-glass and glass ceramic of CaO-SiO_2 system have good bioactivity, being the basis of many bioceramic materials currently in study [3–5]. For instance, calcium silicate ($CaSiO_3$) has revealed great potential in bone restoration because its bending strength is close to the human cortical bone [6], which is higher than the hydroxyapatite (HAp) based ceramics. In vitro tests showed that CaO-SiO_3 (CS) ceramics induce a very high growth of the apatite layer formation in simulated body fluid (SBF), implying the bioactivity of the material [7]. Experiments confirmed that CS ceramics have excellent osteoconduction within 2 weeks of implantation [8]. CS ceramics have faster apatite formation rate (bioactivity) than bioactive glasses in SBF [9], and their ionic dissolution products have been shown they improve cell proliferation and differentiation. In contrast, their very fast degradation, i.e., the high dissolution rate is damaging to cells [10,11], in addition, their mechanical propriety is not ideal [6]. To develop the harmonizing of physical-mechanical and biomedical properties of the CS based ceramics, some elements are added, such as Mg, Ti, Zn, Sr and Zr [12–16]. Studies indicated the incorporation of Mg in CaO–SiO_2–MgO (CMS) ceramics systems may provide greater functionality compared to the CS alone. Mg is an important bioinorganic element in the extracellular matrix of bone, which is essential to cell differentiation and mineralization of bone tissue [16]. Mg can improve osteoblast adhesion and proliferation [17–19], and its deficiency causes osteoporosis [20]. This element also plays an important role decreasing the biodegradation (solubilization) of ceramics [19]. Therefore, CaO–SiO_2–MgO systems ceramics may be used as bioactive materials for bone regeneration. Diopside ($CaMgSi_2O_6$), akermanite ($Ca_2MgSi_2O_7$),

* Corresponding author. Nuclear and Energy Research Institute, Instituto de Pesquisas Energéticas e Nucleares, CCTM (Centro de Ciência e Tecnologia de Materiais), São Paulo, Brazil.
E-mail address: yamagata@ipen.br (C. Yamagata).

https://doi.org/10.1016/j.ceramint.2021.12.169
Received 19 July 2021; Received in revised form 29 November 2021; Accepted 15 December 2021
Available online 18 December 2021

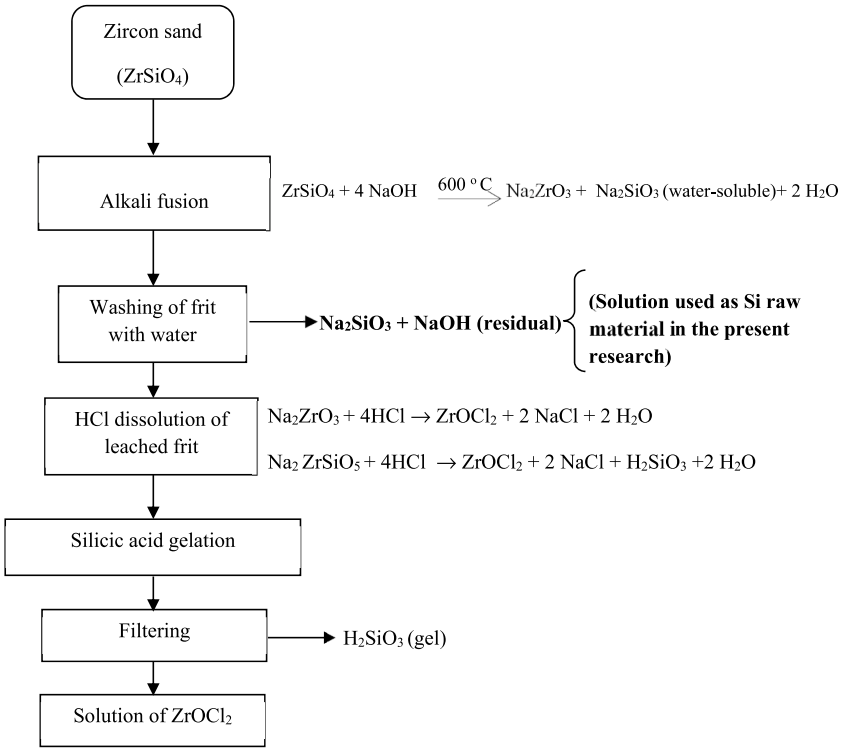

Fig. 1. Alkali fusion process of zircon sand; basic flow chart of the ore opening.

merwinite ($Ca_3MgSi_2O_8$), bredigite ($Ca_7MgSi_4O_{16}$) and monticellite ($CaMgSiO_4$) are crystalline phases belonging to the magnesium containing calcium silicates group [21].

A variety of techniques for bio-glass and glass-ceramic precursor preparation, including solid-state reaction or fusion process [22,23], spray pyrolysis [24], coprecipitation [25,26], and sol-gel [27–29] processes have been reported.

Fusion process consists of heating the precursor elements; silicates and carbonates, at temperatures above 1300 °C, followed by homogenization and cooling [22,23].

In the spray pyrolysis technique of synthesis [24], a solution of salts is atomized through ultrasonic spray generators, into a hot reaction column in which droplets are dried, decomposed, and melted. The glass powders with submicron size, spherical shape and non-aggregated characteristics are obtained at temperatures between 1200 and 1400 °C [24].

Although the solid-state reaction and spray pyrolysis technique of synthesis are straightforward methods, thermal treatment at temperature higher than 1200 °C is required to attain the fixed ceramic crystallization.

Coprecipitation and sol–gel methods are performed from solution medium; therefore, the homogeneity of the components is at the molecular level, giving homogeneous products at comparatively low temperatures. By coprecipitation process, chemically homogeneous crystalline powder can be obtained [25]. Iwata et al. [26] studied sintering behavior and bioactivity of diopside, $CaMgSi_2O_6$, prepared through coprecipitation. As-prepared powder was synthesized by adding aqueous ammonia to an ethanol solution containing Ca $(NO_3)_2{\cdot}4H_2O$, Mg $(NO_3)_2{\cdot}6H_2O$, and Si $(OC_2H_5)_4$. The dried powder was X-ray amorphous and crystallized into diopside at 845.5 °C.

In the sol-gel method, the product is derived from hydrolysis and gelation of alkoxides mixed with metal salts [27–29]. It is performed at room temperature that consists in advantages of the route, added to better control of the composition, obtaining of materials with high surface area and good structural homogeneity [30]. Despite these advantages, the method is time consuming (about one week) [31], costly, and the precursor materials (metal alkoxides) are toxic. Due to the high price of silicon alkoxides, the production of glass via the sol−gel process costs 100 times [30] that of glass obtained via conventional silica melting and cast. Therefore, the process is only economically viable for obtaining high value-added products. Precursor materials used in a typical sol-gel process are commercial oxides (CaO, MgO) or nitrate salts ($Ca(NO_3)_2{\cdot}4H_2O$, Mg $(NO_3)_2{\cdot}6H_2O$)) and commercial SiO_2 or Si $(OC_2H_5)_4$ (tetraethyl orthosilicate - TEOS).

The objective of this work is to report a novel cost-effective synthesis of bioceramic powder of CaO–SiO_2–MgO systems using a waste solution as source of silica, instead of TEOS; a reagent usually employed which is expensive and toxic. The novel procedure combines sol-gel and coprecipitation techniques. Ceramic powder of CaO–SiO_2–MgO systems was synthesized from Na_2SiO_3 solution (used in synthesis route I and synthesis route II) and conventional sol-gel from TEOS (used in synthesis route III). Na_2SiO_3 solution used as source of Si is a waste matter derived from alkaline fusion process of zircon sand [32]. In the synthesis route I and synthesis route II, hydrochloric acid was added to sodium silicate solution resulting in gel of silica under acidic and basic setting catalysis reaction, respectively. Ca^{2+} and Mg^{2+} ions were co precipitated with NaOH as respective hydroxides. The co precipitated hydroxides were mixed with gel of silica. The resulted mixture was submitted to processing of filtering, drying, washing and thermal treatment to obtain ceramic precursor powder. The conventional sol-gel method was performed to synthesize the same ceramic powder using TEOS as raw material (synthesis route III). The characteristics of the synthesized products obtained through three routes were presented. The proposed routes of synthesis substantially shortened the synthesis time since the gel formation was reached in 72h for synthesis route I and few minutes in synthesis route II. The use of Na_2SiO_3, a low-cost raw material for silica, showed satisfactory results and it may be an attractive substitute for the traditional TEOS, a high-cost reagent.

Table 1
Nominal composition of synthesized ceramic powders.

Components	Mass (%)
SiO_2	49.30
CaO	43.19
MgO	7.68

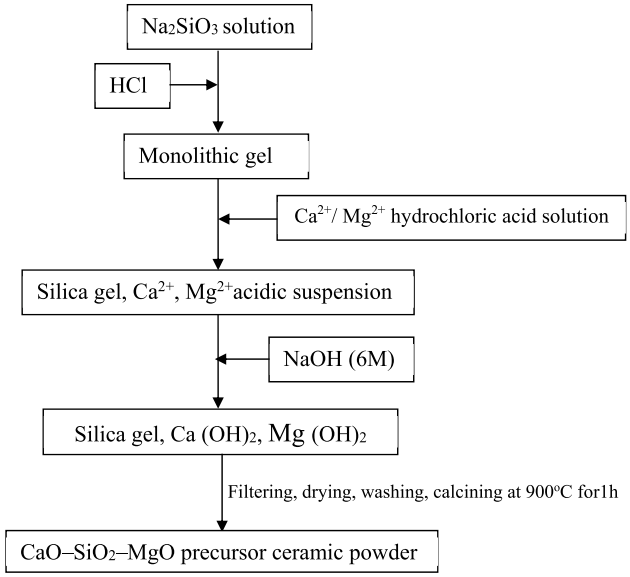

Fig. 2. Flowchart of the synthesis process I; sol-gel method combined with coprecipitation using Na_2SiO_3 and acidic pH.

2. Materials and methods

2.1. Obtaining of Na_2SiO_3 starting solution from alkaline fusion process of zircon sand

Fig. 1 shows a basic flowchart of alkali fusion process of zircon sand to ore opening [32] for obtaining Na_2SiO_3 solution.

The process was performed at 600 °C for 2h, at that time the reaction of alkaline fusion of zircon sand takes place and caustic frit is formed, which is a mixture of sodium zirconate and sodium silicate. This frit was washed with water (5 times the volume of the frit) to remove the water-soluble sodium silicate. In the present work, the water-leached solution (water soluble sodium silicate) was used as raw material of Si.

2.2. Synthesis process

The precursor of Si used was sodium silicate solution, water-leached solution from alkaline fusion process of zircon sand. The solution was obtained as described in item *2.1*. Hydrochloric solutions of calcium and magnesium were used as sources of Ca and Mg, achieved by dissolution of the respective oxides in 2 M, HCl.

The nominal composition of synthesized ceramic powders is shown in Table 1.

2.2.1. Synthesis process I - sol-gel combined with coprecipitation using Na_2SiO_3 as precursor of Si, and acidic pH

Initially, HCl (3 M) solution was slowly added, under mechanical stirring, to a beaker containing Na_2SiO_3 solution up to acidic pH (~pH of 2). After a 72h rest, a monolithic silica gel was obtained. Subsequently, the gel and hydrochloric acid solutions of Ca^{2+} and Mg^{2+} were mixed to obtain a suspension of the gel and cations. Then, under mechanical stirring, NaOH solution (6 M) was added up to pH 10 for coprecipitation of Ca and Mg hydroxides. The resulting suspension of gel and hydroxides was filtered, dried at 70 °C for 24h, washed with deionized water until negative test for Cl^- and calcined at 900 °C for 1 h to obtain precursor ceramic powder. The sample was denoted as SAS (synthesis, acid, sodium silicate) sample. Fig. 2 displays the flowchart of the synthesis process I; sol-gel method combined with coprecipitation using Na_2SiO_3 and acidic pH.

2.2.2. Synthesis process II - synthesis by sol-gel method combined with coprecipitation using Na_2SiO_3 solution as source of Si and basic pH

Na_2SiO_3 solution was mixed with 10% volume ethanol. The pH of Na_2SiO_3 solution is highly alkaline, i.e., close to the pH of 14, as it has residual NaOH (see Fig. 1). Thus, HCl solution (3 M) was slowly added under mechanical stirring, until reaching the basic pH of 10, which was verified with pH meter. In a few minutes there was the formation of silica gel.

A mixture of Ca^{2+} and Mg^{2+} hydrochloric acid solutions was slowly added to a beaker containing NaOH (6 M), under constant stirring, for precipitation of Ca^{2+} and Mg^{2+} hydroxides at pH of 10. This resultant solution containing precipitates of Ca and Mg hydroxides were mixed with the above formed silica gel, and then, this mixture was homogenized for 20 min by energetic mechanical stirring. Then, it was filtered, dried at 70 °C for 24 h, washed with deionized water until negative test for Cl^- and calcined at 900 °C for 1h to obtain the precursor ceramic powder. The sample was denoted as SBS (synthesis, basic, sodium silicate). Fig. 3 shows the flowchart of the synthesis process II; sol-gel method combined with coprecipitation using Na_2SiO_3 and basic pH.

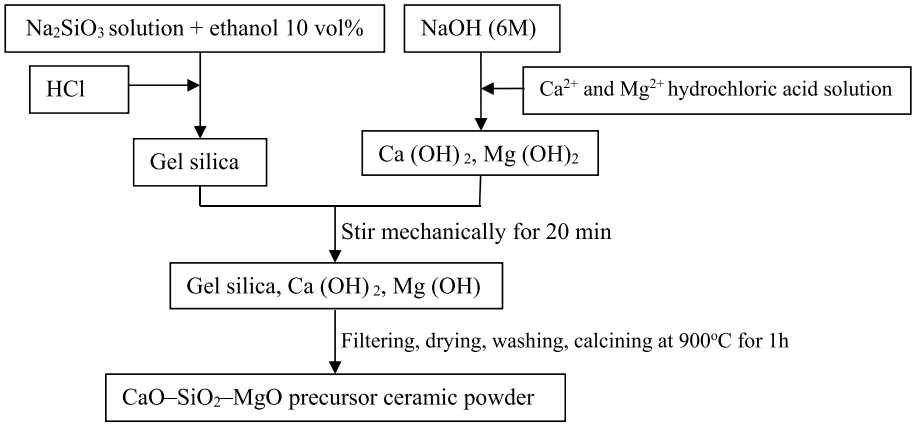

Fig. 3. Flowchart of the synthesis process II; sol-gel method combined with coprecipitation using Na_2SiO_3 and basic pH.

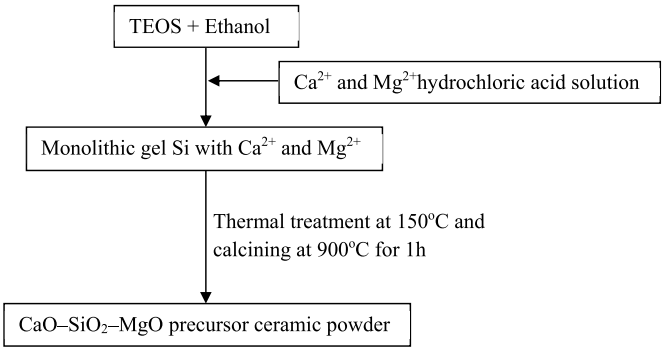

Fig. 4. Flowchart of the synthesis process III; sol-gel method using TEOS and acidic pH.

2.2.3. Synthesis process III- synthesis by sol-gel method using TEOS, as a precursor of Si, and acidic pH

In a beaker, TEOS was mixed with ethanol in the volume ratio of 1:1. The hydrochloric acid solution of Ca^{2+} and Mg^{2+} was slowly added, under constant stirring, in the beaker. Then, it was left at rest and after 6 h; a monolithic gel of silica containing Ca^{2+} and Mg^{2+} was produced. Afterward, this gel was thermal treated on a hot plate (~150 °C) and calcined at 900 °C for 1h, to obtain the precursor ceramic powder. The sample was denoted as SAT (synthesis, acid, TEOS). Fig. 4 shows the flowchart of the synthesis process III; sol-gel method using TEOS and acidic pH.

2.2.4. Processing of ceramic powder for obtaining ceramic body

The precursor ceramic powder was compacted in a cylindrical matrix of 15 mm in diameter in hydraulic press using pressure of $2.49 \cdot 10^7$ Pa. The obtained compact was sintered in an electric oven at 1200 °C for 2 h, with heating rate of 10 °C·min^{-1}. The sintered ceramic body was used for cytotoxicity and bioactivity in vitro testing.

2.3. Characterization

2.3.1. X-ray diffraction

The X-ray diffraction technique was applied to analyze the obtained crystalline phases in ceramic powder and sintered samples, using a Multiflex model diffractometer from Rigaku, with a source of monochromatic radiation CuKα (λ = 1.54148 Å). The analyses were performed with a step of 0.06°, in the angular range $10° \leq 2\theta \leq 90°$ and counting time of 4s per step. The Crystallographic Search Match

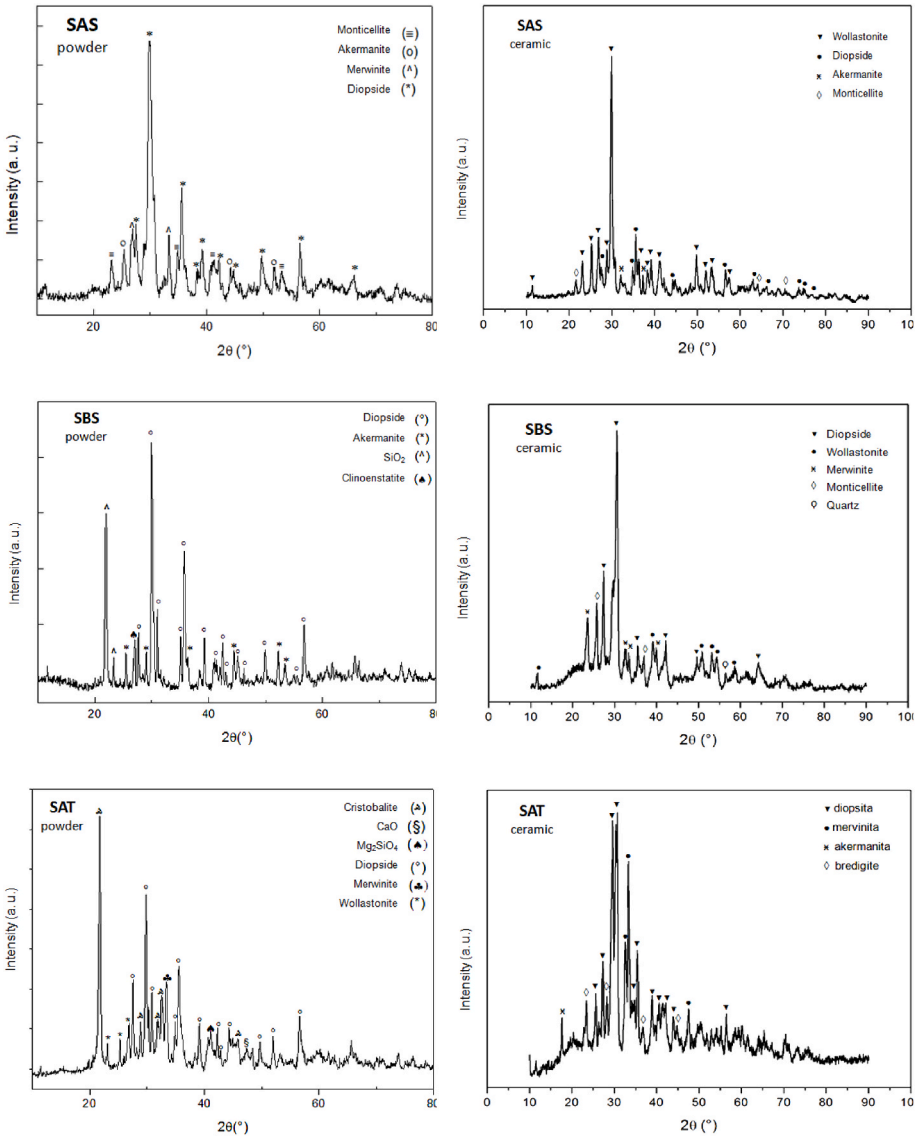

Fig. 5. XRD patterns of SAS, SBS and SAT powders calcined at 900 °C for 1h and XRD patterns of SAS, SBS and SAT ceramic body sintered at 1200 °C for 2h.

Table 2
Main crystalline phase of ceramic samples.

Sample	Precursor of Si	Main crystalline phase
SAS	Na_2SiO_3	Wollastonite
SBS	Na_2SiO_3	Diopside
SAT	TEOS	Diopside, merwinite

software was used to identify crystalline phases by qualitative interpretation. The peaks displayed in the XRD pattern of the samples were compared with the database patterns from the ICDD (The International Centre for Diffraction Data). Following the model adopted by Choudhary et al. [33], the main phase of each sample was qualitatively indicated.

2.3.2. *In vitro cytotoxicity tests*

The cytotoxicity of samples SAS, SBS and SAT were investigated, as the first biological test recommended by the ISO10993-1:2018. The test was standardized according to ISO 10993-5:2009 at Biotechnology Centre of Nuclear and Energy Research Institute – Brazil, by indirect method, which involved the preparation of cell and sample as following. The 3T3/NIH (ATCC® CRL 1658) fibroblasts were cultured with DMEM (Dulbecco-modified Eagle culture medium - Invitrogen) supplemented with 10% FBS (fetal bovine serum – Athená Biotecnologia) and 1% antibiotic/antimitotic solution (Invitrogen) in an incubator at 37 °C with 5% carbon dioxide (CO_2). They were grown to 80% confluence in a culture treated flask and detached with an EDTA/trypsin solution (Sigma). The cells in suspension were counted in a Neubauer chamber and seeded in a 96-well plate or subcultured. For sample preparation, the recommendations of the ISO10993-12:2021 were followed. The samples were initially sterilized in an autoclave (at 121 °C for 15 min – humid heat) and after that, all procedures were done in laminar flow. Then the samples were immersed in supplemented culture medium for NIH/3T3 cells in the ratio 3 cm^2 mL^{-1} in a sterile tube for each sample. The tubes with the sample and the culture medium were placed in a water bath at 37 °C for 72h under kind stirring to obtain the sample extract. For cytotoxicity test, a 96-well plate was seeded with 2 x 10^4 cells NIH/3T3 per well in 10 out of 12 columns for 24h in an incubator at 37 °C and 5% carbon dioxide (CO_2). Then, the medium of each well was changed by the extract samples from SAS, SBS, SAT, the material of interest; and alumina as a negative reference material; latex as a positive reference material; and supplemented culture medium as 100% of cell viability - control. The extract was pipetted onto a column (n=8), for another 24h in the incubator. After the second incubation, the extracts were aspirated and pipetted to the new culture medium culture medium

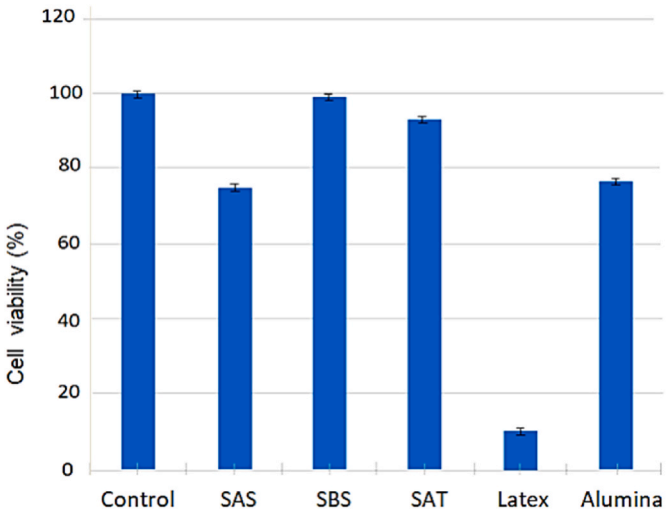

Fig. 7. Results of indirect cytotoxicity test of the cell viability assay of SAS, SBS and SAT.

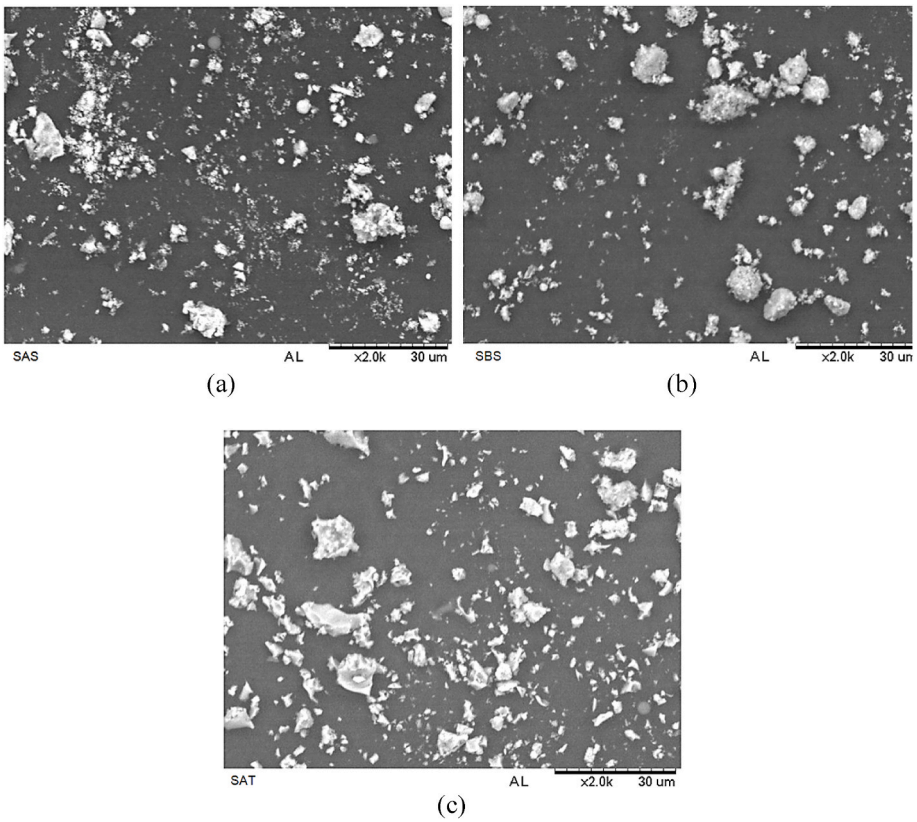

Fig. 6. Scanning electron micrograph of SAS (a), SBS (b) and SAT (c) powder, calcined at 900 °C for1h.

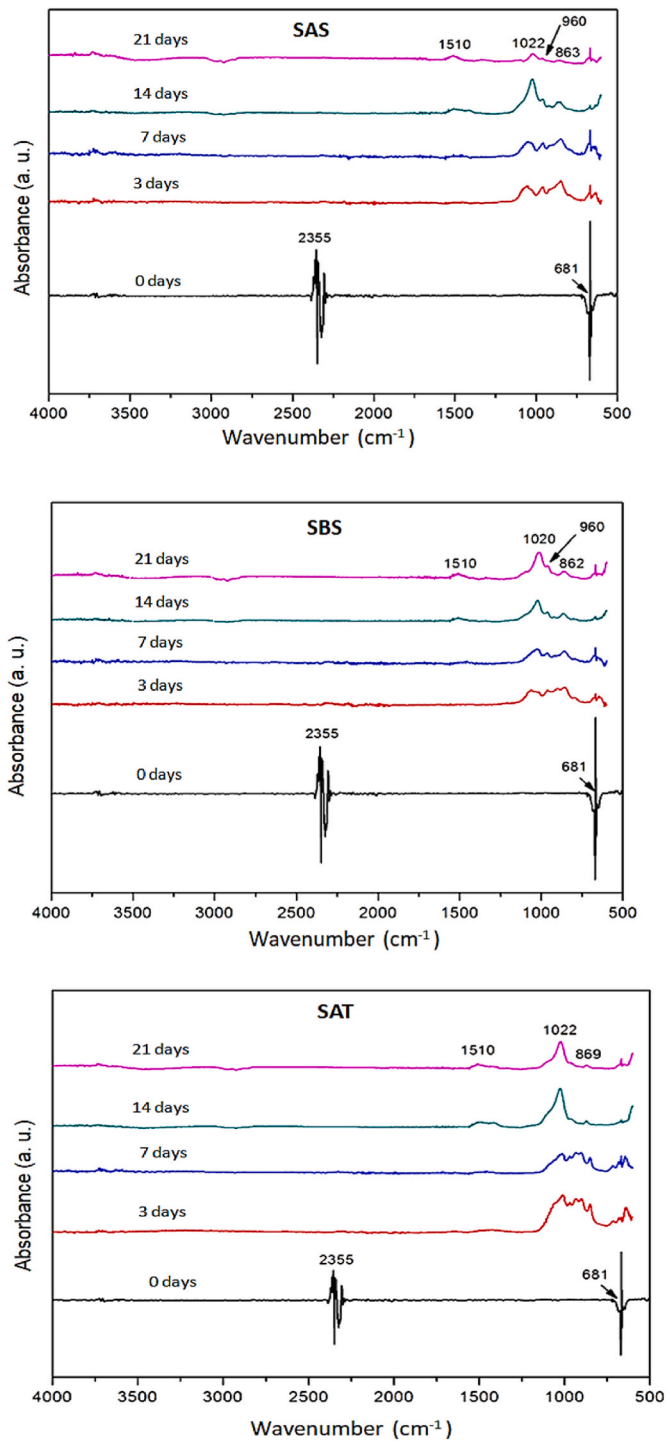

Fig. 8. FTIR spectra of SAS, SBS and SAT sintered surface, before and after soaking in SBF for 3, 7, 14 and 21 days.

with 3-(4,5-dimethylthiazol-2-yl)-5-(3-carboxymethoxyphenyl)-2-(4-sulfophenyl)-2H-tetrazolium (MTS) MTS (Promega) and incubated again for 2 h in the incubator. Colorimetric measurement was performed in a spectrophotometer at 490 nm. Cell viability was calculated by the following equation:

$$CV(\%) = \frac{ODc}{ODs} \times 100$$

Where: CV = cell viability, ODc = optical density - control, ODs = optical density - sample.

2.3.3. In vitro bioactivity evaluation (hydroxyapatite formation)

To verify the hydroxyapatite (HAp) formation ability on the surface of sintered ceramics, they were soaked in simulated body fluid (SBF) at solid (S) to liquid (L) loading of $1 \cdot 100^{-1}$ (g mL^{-1}) and then kept at 37 °C for 3, 7, 14 and 21 days. SBF solution was prepared according to the procedure described by Kokubo et al. [34]. Hydroxyapatite deposition on the surface of the samples, after immersion in SBF, was established by Fourier infra-red technique, performed in a frequency range of 500–4000 cm^{-1} (Thermo Scientific Nicolet 6700 FT-IR). The surface morphology and microstructure of the samples, after soaking in the SBF, were also observed by SEM.

3. Results and discussion

In Fig. 5, XRD patterns of SAS, SBS and SAT powders calcined at 900 °C for 1h and XRD patterns of SAS, SBS and SAT ceramic body sintered at 1200 °C for 2h are shown.

From XRD patterns shown in Fig. 5, it is observed that the SAS, SBS and SAT powder samples show multi crystalline phases. The pattern of the SAS powder presents the crystalline phases: diopside (ICDD 75-1092), akermanite (ICDD 35-592), merwinite (ICDD 35-591) and monticellite (ICDD 35-590), with high proportion of diopside. SBS powder sample pattern shows the crystalline phases: diopside (ICDD 75-1092), akermanite (ICDD 35-592), silicon oxide (ICDD 51-1379) and clinoenstatite (ICDD 75-1406). Diopside is the main phase. The presence of free SiO_2 observed in SBS powder sample may indicate that the mixture of Ca $(OH)_2$, Mg $(OH)_2$ with silica gel in the process (Fig. 3) was not as much as necessary to obtain an adequate homogeneity of the components. Increasing the mixing time might improve the homogeneity and the presence of SiO_2 in calcined powder will possibly be prevented. SAT powder sample presents the phase: wollastonite (ICDD 73-11 10), diopside (ICDD 75-1092), merwinite (ICDD 35-591), magnesium silicate (ICDD 74-1684), calcium oxide (ICDD 3-865) and cristobalite (ICDD 82-512). The cristobalite phase is the predominant. In the process of obtaining this sample (Fig. 4), a monolithic silica gel is formed by the addition of Ca^{2+} and Mg^{2+} hydrochloric solution in the solution containing TEOS and ethanol. In this gel the ions (Ca^{2+} and Mg^{2+}) were distributed homogeneously, so homogeneity is expected to be preserved through processing. However, the presence of CaO and cristobalite (SiO_2) are confirmed in the spectra. Segregation of these oxides, probably, occurred during the heat treatment of the sample at 150 °C.

Fig. 5 shows that crystalline phases such as diopside, akermanite, merwinite, monticellite and wollastonite, were obtained in the synthesized powder samples. Clinoenstatite, cristobalite, magnesium silicate, silicon oxide and calcium oxide present in the SBS or SAT powders might be transformed into desired crystalline phases (diopside, akermanite, merwinite, monticellite and wollastonite) by the sintering process. In the XRD pattern of SAS ceramic sample, Wollastonite, monticellite, diopside and akermanite phases are observed, according to: PDF No. 76-186, PDF No.35-590, PDF No. 83-1817 and PDF No.87-50, respectively. It was found that the wollastonite is the main phase while the others are secondaries. Wollastonite (PDF No.76-186), diopside (PDF No.83-1817), merwinite (PDF No.35-591), monticellite (PDF No.35-590) and quartz (PDF No.86-1562) are observed in SBS ceramic sample. Remarkably diopside is the main crystalline phase and the others are secondaries. In sintered SAT ceramic sample, it is observed the diopside, merwinite, akermanite and bredigite phases, according to: PDF No.83-1817, PDF No.35-591, PDF No.87-50 and PDF No.36-399, respectively. The main crystalline phases are diopside and merwinite.

Table 2 shows the relationship of the main crystalline phases of ceramic samples.

All sintered ceramic samples presented multi crystalline phases, among them; diopside [35], akermanite [36], merwinite [37], monticellite [38] and wollastonite [39]. According to the literature, all those crystalline phases indicate they have the bioactivity property, since they induce the formation of hydroxyapatite on the ceramic body in SBF

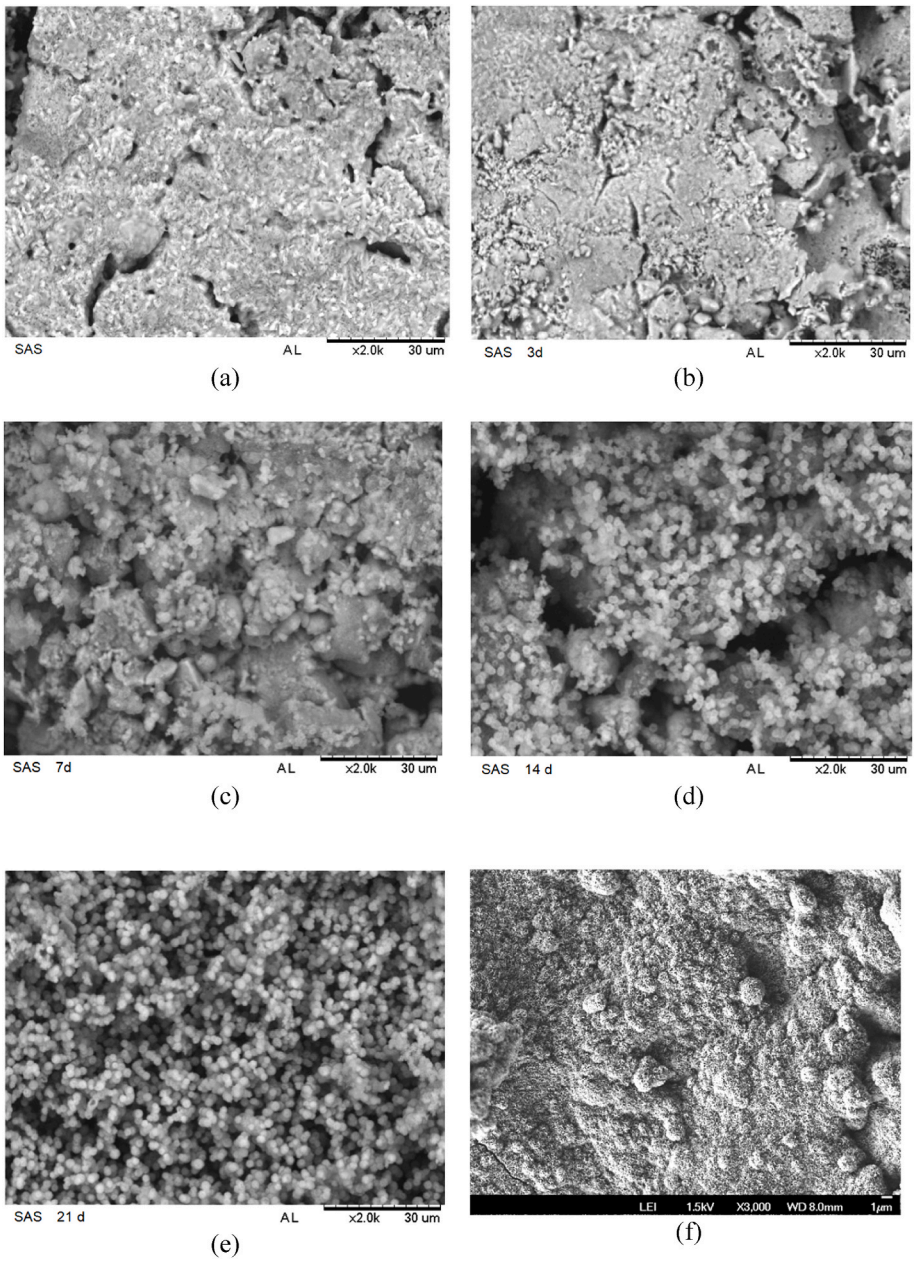

Fig. 9. SEM micrographs of sintered SAS ceramic sample surface, before (a) and after soaking in SBF for 3 (b), 7 (c), 14 (d) and 21 (e, f) days.

solution. In addition, they also present good rate of osteoblast stake on the surface of the ceramic, indicating their biocompatibility.

Scanning electron micrograph of SAS, SBS and SAT powders calcined at 900 °C for 1h are shown in Fig. 6.

It is observed that the samples SAS powder (Fig. 6 (a)) and SBS powder (Fig. 6 (b)) present agglomerates (<30 μm) which are porous like and constituted by rounded morphology particles smaller than 3 μm. In Fig. 6(c), hard-looking clusters smaller than 30 μm with irregular morphology particles are observed in the sample SAT powder.

In Fig. 7, the plotted column shows the result of the indirect cytotoxicity test, whose cell viability assay selected molecules, obtained from the liquid extract of the samples, which have toxic effects on fibroblast proliferation and eventually leads cell death. Fibroblast (control), negative reference material alumina (non-cytotoxic) and positive latex reference (cytotoxic) were used as parameters to determine the concentration of cells that were dead due to contact with possibly toxic molecules present in the liquid extract.

In Fig. 7, it is observed that the cellular viability of the SAS sample is above 70%. It was greater than 90% for the SBS and SAT samples. According to ISO 10993-5:2009 [40], in which the cytotoxicity parameter in the indirect test is defined; it specifies a cell survival rate greater than or equal to 70%, for the test to be considered appropriate. Thereby, the samples SAS, SBS and SAT can be considered non cytotoxic, that is the first criterion analyzed for continuing investigate their biocompatibility.

The integration and binding of bioactive material to living bone is achieved by the formation of Hap layer on the surface of this material when it is implanted. The presence of bone-like Hap layer is considered predictive of bioactivity of the material in vivo. This apatite formation behavior, however, depends on several factors, such as the chemical composition, the crystalline phase, the surface chemistry, the solubility, the porosity, the morphology of the powder, the microstructure of ceramics etc. The in vitro indicator of the bone-bonding ability of materials can be recognized in simulated body environment Kokubo's SBF [41]. Although this approach has been discussed over the last decade, and that in vitro conditions may not be the exact same in vivo, the test remains important for medical implants, which is widely accepted by materials

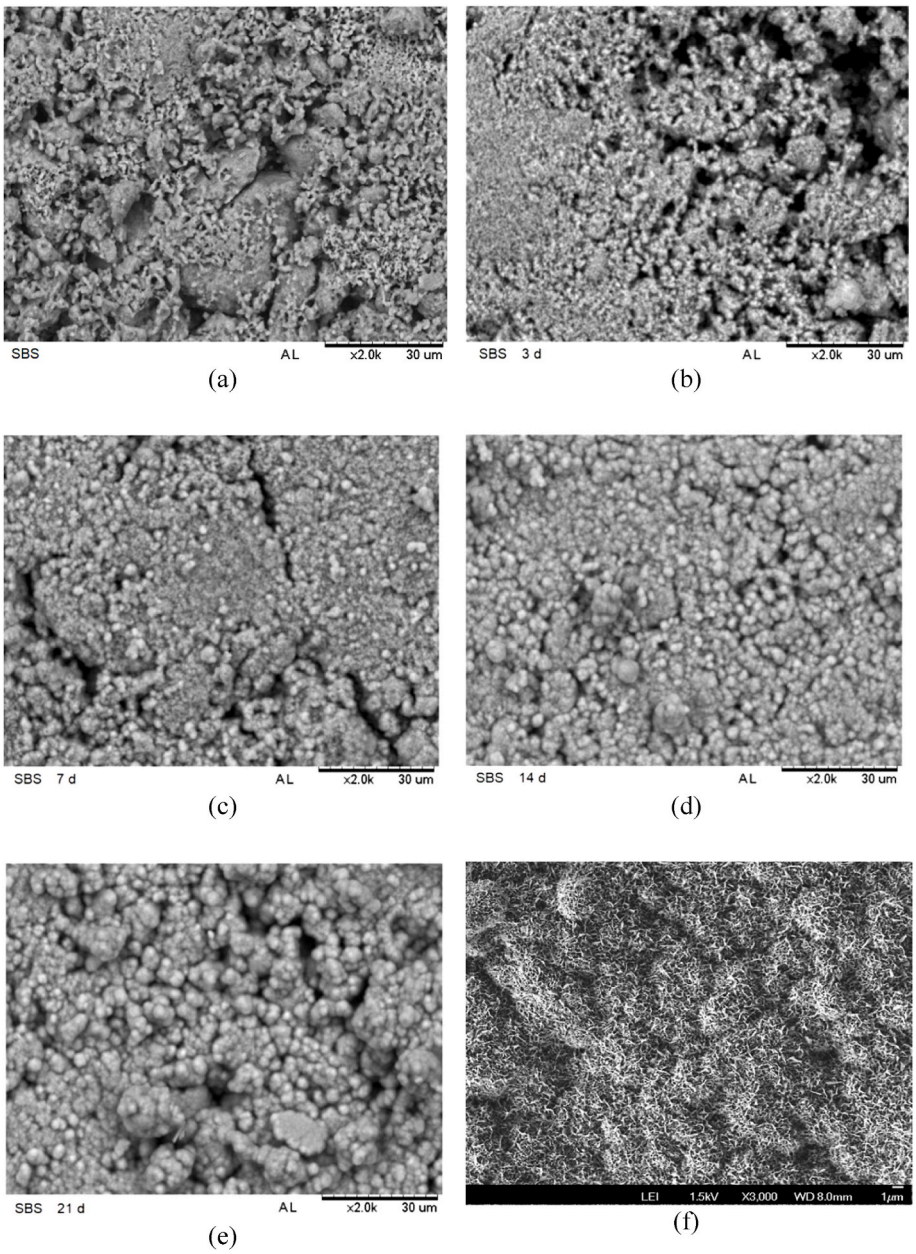

Fig. 10. SEM micrographs of sintered SBS ceramic sample surface, before (a) and after soaking in SBF for 3 (b), 7 (c), 14 (d) and 21 (e, f) days.

researchers [41], and it might help to predict the bioactivity of biomedical materials. We investigated the apatite formation behavior on prepared ceramic samples under in vitro condition using SBF developed by Kokubo [34]. The presence of Hap on the surface of samples was cheeked using FTIR (Fourier transform infrared) analysis. FTIR spectroscopy analysis of sintered SAS, SBS and SAT samples, before and after soaking in SBF for 3, 7, 14 and 21 days are shown in Fig. 8.

In Fig. 8 it is verified that the spectra presented by the samples are very similar. In these figures, in the curve indicating 0 days, it is observed the presence of a typical silica related band with frequency around 2300 cm^{-1} and a less intense peak in the region of 650 cm^{-1}, which agree with the literature [42,43]. The first region corresponds to the silanol linkage, while the second region is assigned to the siloxane linkage. Typical bands might indicate the presence of hydroxyapatite [44] in the spectra, i.e., when peaks of infrared absorption between 1000 and 1100 cm^{-1} that can be attributed to $(PO_4)^{3-}$ bond, and between 1380 and 1580 cm^{-1} attributed to $(CO_3)^{2-}$ bond [9,45] are verified. According to Slósarczyk et al. [45] groups $(CO_3)^{2-}$ and $(PO_4)^{3-}$ also have mild peaks of approximately 870 cm^{-1} and 963 cm^{-1}, respectively. The presence of typical bands that can be attributed to hydroxyapatite, is observed. This is clear for the samples after soaking 14 and 21 days in SBF. Those results show that the samples SAS, SBS and SAT have apatite-formation ability in the simulated body fluid, and this might indicate their bioactivity.

Micrographs obtained by SEM of sintered SAS ceramic sample surface are shown in Fig. 9, before (Fig. 9(a)) and after soaking in SBF for 3 (Fig. 9(b)), 7 (Fig. 9(c)), 14 (Fig. 9(d)) and 21 (Fig. 9(e) and (f)) days.

Fig. 9(a) (SAS sintered ceramic sample) and Fig. 9(b) (sample 3d soaked) are not significantly different from one another, the presence of hydroxyapatite was not verified on both, i.e., in Fig. 8, the typical absorption peak at 1022 cm^{-1} attributed to the group $(PO_4)^{3-}$ was not present in spectra of the samples. In Fig. 9(c) (sample 7d soaked) it is possible to observe the presence of few rounded morphology particles that could be attributed to hydroxyapatite on the sample surface, but its presence is not obvious in the FTIR spectrum in Fig. 8. In Fig. 9(d) (sample 14d soaked), a significant amount of rounded morphology

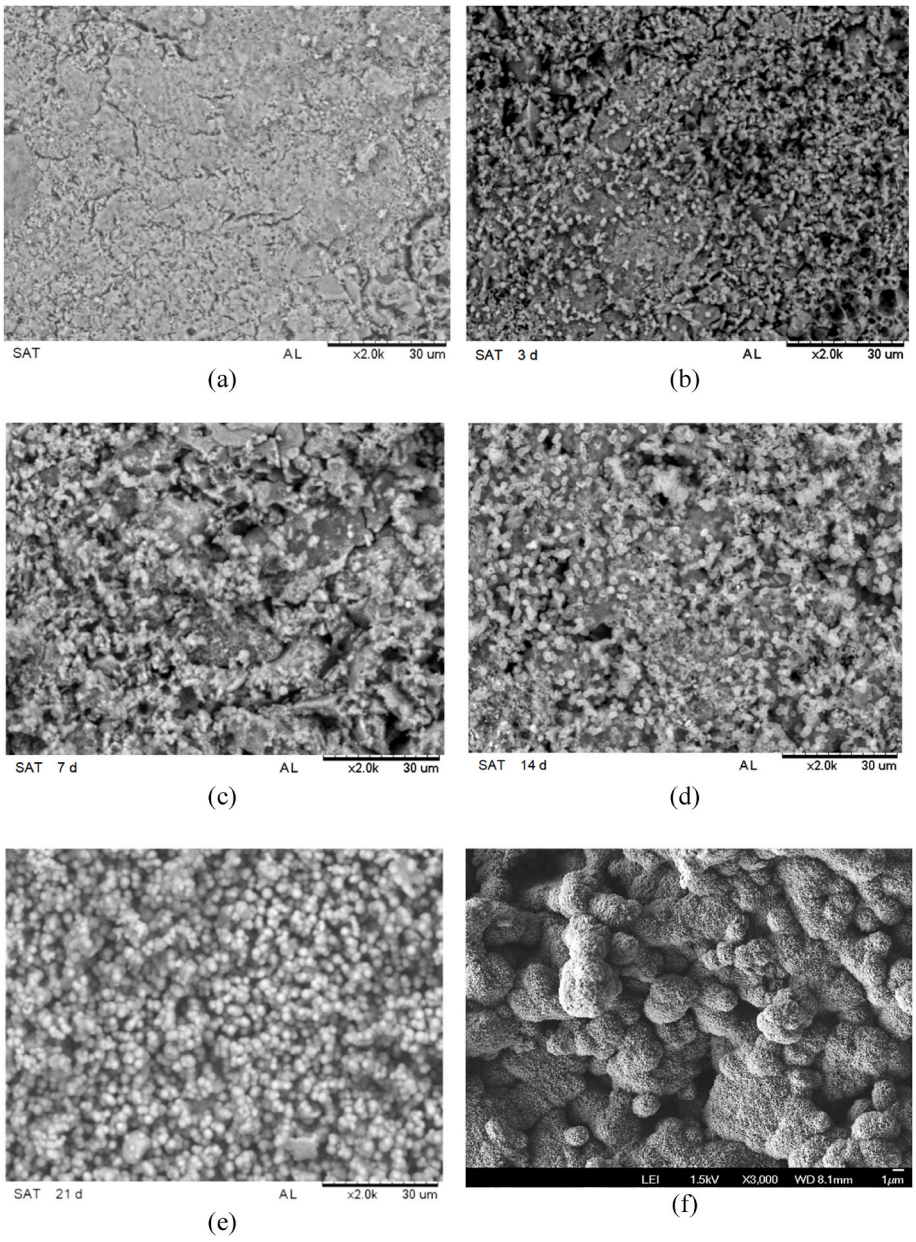

Fig. 11. SEM micrographs of sintered SAT ceramic sample surface, before (a) and after soaking in SBF for 3 (b), 7 (c), 14 (d) and 21 (e, f) days.

particles is observed, and it is even greater in Fig. 9(e). In high magnification micrograph (Fig. 9(f)) the surface of ceramic sample (Fig. 9(a)) cannot be seen, as a result the substrate was completely covered. The morphology of these particles suggests they might be hydroxyapatite. This can be confirmed by the results shown in Fig. 8, where the presence of typical hydroxyapatite bands is observed in the samples after soaking by 14d (Figs. 9(d) and 21d (Fig. 9(e, f)). Therefore, the SAS sample can form hydroxyapatite on the surface from 14 days of soaking in SBF.

Fig. 10 presents SEM micrographs of the sintered SBS ceramic sample surface before (Fig. 10(a)) and after immersion in SBF for periods of 3 (Fig. 10(b)), 7 (Fig. 10(c)), 14 (Fig. 10(d)) and 21 (Fig. 10(e) and (f)) days.

The micrographs shown in Fig. 10 are like those shown in Fig. 9. Comparing the images in Fig. 10(a) and (b) it is not possible to observe any substantial difference. In Fig. 10(c) it can be verified that the sample surface is covered by rounded morphology particles. As previously commented, the presence of these particles is indicative of hydroxyapatite (peak absorption at 1022 attributed to PO_4^{3-} group) which can be confirmed by the results obtained by FTIR shown in Fig. 8. The hydroxyapatite layer gradually became more compact from Fig. 10(c), followed by Fig.10(d) to Fig.10(e). In Fig. 10(d) and (e) the surfaces are completely covered by a dense apatite layer. Particles with worm-like morphology, which is typical of hydroxyapatite, are observed in high magnification micrographs shown in Fig. 10(f).

Fig. 11 presents micrograph obtained by SEM from the surface of sintered SAT ceramic sample before Fig. 11(a)) and after immersion in SAT for periods of 3 (Fig. 11(b)), 7 (Fig. 11(c)), 14 (Fig. 11(d)) and 21 (Fig. 11(e) and (f)) days.

Comparing the images of Fig. 11(a) and (b) (immersion in SBF by 3d) it is possible to notice in the latter, the presence of small, rounded morphology particles. According to Fig. 8 they were identified as hydroxyapatite (peak absorption at 1022 cm^{-1} attributed to $(PO_4)^{3-}$ group). There is no significant difference between Fig. 11(c) and (d), but there was a gradual growth in the size and volume of these particles, from the 3d soaked sample to the 21d soaked sample as shown in Fig. 11 (e). In Fig. 11(f) there is high magnification surface image of 21 soaked

sample; a very dense layer of hydroxyapatite can be highlighted.

4. Conclusions

This work reported three routes for the synthesis of the bioceramic powder of the CaO-MgO-SiO_2 system. Two processes of synthesis were proposed from Na_2SiO_3. The first was performed in acidic pH and the other in basic pH medium. Both processes combined the sol-gel and coprecipitation techniques. The conventional sol-gel method from TEOS was also presented. In the proposed route from Na_2SiO_3 in acidic pH, the time of silica gel formation was of 72h. This time is substantially short than those reported by others researches that employ the traditional polymer sol-gel synthesis in which the metal alkoxides are used as precursor of silica and therefore a prolonged hydrolysis step is required. In the route from Na_2SiO_3 in basic pH, the gel-formation occurred within few minutes. It is important to highlight that in these two synthesis routes, Na_2SiO_3 was used instead of TEOS. TEOS, which is traditionally used in the conventional sol-gel process, is a high toxicity and expensive reagent.

Ceramic bodies obtained from synthesized bioceramic powders, and sintered at 1200 °C for 2h, presented multi crystalline phases, mainly diopside and wollastonite.

The in vitro cytotoxicity test has shown that, all ceramic samples can be considered no cytotoxic. The cell viability was greater than 70% that characterizes a great potential for biocompatibility of samples. FTIR spectroscopy and SEM micrographs demonstrated that those ceramics have apatite-formation ability after 14 days soaking in SBF. After 21 days of soaking, the surface of these ceramic samples, were completely covered with hydroxyapatite.

Finally, the sol gel method combined with coprecipitation, which to our knowledge is not found in the literature, can be applied for synthesis of other silicate based ceramic powders.

Declaration of competing interest

The authors declare that they have no known competing financial interests or personal relationships that could have appeared to influence the work reported in this paper.

Acknowledgments

This project was funded from The São Paulo Research Foundation, (FAPESP) through the project FAPESP nº: 2018/10114-7. The authors thank Zilda Ribeiro Coninck for the correction of English.

References

[1] A. Hoppe, N. S. Güldal, A. R. Boccaccini, A review of the biological response to ionic dissolution products from bioactive glasses and glass-ceramics, Biomaterials, vol. 32, nº 11, p. 2757–2774, abr. 2011, doi: 10.1016/j.biomaterials.2011.01.004.

[2] Department of Cranio-Maxillofacial Surgery, University of Münster, Waldeyerstr. 30, D-48149 Münster. Germany U. Meyer, A. Büchter, H. Wiesmann, U. Joos, D. Jones, Basic reactions of osteoblasts on structured material surfaces, Eur. Cell. Mater. 9 (2005) 39–49, https://doi.org/10.22203/eCM.v009a06. abr.

[3] K. Łukowicz, et al., The role of CaO/SiO_2 ratio and P_2O_5 content in gel-derived bioactive glass-polymer composites in the modulation of their bioactivity and osteoinductivity in human BMSCs, Mater. Sci. Eng. C 109 (2020), 110535, https://doi.org/10.1016/j.msec.2019.110535 abr.

[4] S. Koppala, et al., Sol gel combustion derived monticellite bioceramic powders for apatite formation ability evaluation, Mater. Res. Express 6 (12) (2020), 125431, https://doi.org/10.1088/2053-1591/ab8256 abr.

[5] H.C. Li, et al., Microstructure, mechanical and biological properties of laser cladding derived CaO-SiO_2-MgO system ceramic coatings on titanium alloys, Appl. Surf. Sci. 548 (2021), 149296, https://doi.org/10.1016/j.apsusc.2021.149296 may.

[6] K. Lin, W. Zhai, S. Ni, J. Chang, Y. Zeng, W. Qian, Study of the mechanical property and in vitro biocompatibility of $CaSiO_3$ ceramics, Ceram. Int. 31 (2) (2005) 323–326, https://doi.org/10.1016/j.ceramint.2004.05.023, jan.

[7] Y. Iimori, Y. Kameshima, A. Yasumori, K. Okada, Effect of solid/solution ratio on apatite formation from $CaSiO_3$ ceramics in simulated body fluid, J. Mater. Sci. Mater. Med. 15 (11) (2004) 1247–1253, https://doi.org/10.1007/s10856-004-5888-0, nov.

[8] Y.-J. Seol, K.-H. Kim, I.A. Kim, S.-H. Rhee, Osteoconductive and degradable electrospun nonwoven poly(ε-caprolactone)/CaO-SiO_2 gel composite fabric, J. Biomed. Mater. Res. A 9999A (2010), https://doi.org/10.1002/jbm.a.32738. NA-NA.

[9] P. Siriphannon, Y. Kameshima, A. Yasumori, K. Okada, S. Hayashi, Formation of hydroxyapatite on $CaSiO_3$ powders in simulated body fluid, J. Eur. Ceram. Soc. 22 (4) (2002) 511–520, https://doi.org/10.1016/S0955-2219(01)00301-6, abr.

[10] Y. Iimori, Y. Kameshima, K. Okada, S. Hayashi, Comparative study of apatite formation on $CaSiO_3$ ceramics in simulated body fluids with different carbonate concentrations, J. Mater. Sci. Mater. Med. 16 (1) (2005) 73–79, https://doi.org/10.1007/s10856-005-6449-x, jan.

[11] C. Wu, Methods of improving mechanical and biomedical properties of Ca–Si-based ceramics and scaffolds, Expet Rev. Med. Dev. 6 (3) (2009) 237–241, https://doi.org/10.1586/erd.09.3, may.

[12] C. Wu, J. Chang, J. Wang, S. Ni, W. Zhai, Preparation and characteristics of a calcium magnesium silicate (bredigite) bioactive ceramic, Biomaterials 26 (16) (2005) 2925–2931, https://doi.org/10.1016/j.biomaterials.2004.09.019, jun.

[13] C. Wu, Y. Ramaswamy, X. Liu, G. Wang, H. Zreiqat, Plasma-sprayed $CaTiSiO_5$ ceramic coating on Ti-6Al-4V with excellent bonding strength, stability and cellular bioactivity, J. R. Soc. Interface 6 (31) (2009) 159–168, https://doi.org/10.1098/rsif.2008.0274, fev.

[14] D. Boyd, G. Carroll, M.R. Towler, C. Freeman, P. Farthing, I.M. Brook, Preliminary investigation of novel bone graft substitutes based on strontium–calcium–zinc–silicate glasses, J. Mater. Sci. Mater. Med. 20 (1) (2009) 413–420, https://doi.org/10.1007/s10856-008-3569-0, jan.

[15] H. Jodati, B. Yilmaz, Z. Evis, Calcium zirconium silicate (baghdadite) ceramic as a biomaterial, Ceram. Int. 46 (14) (2020) 21902–21909, https://doi.org/10.1016/j.ceramint.2020.06.105, oct.

[16] C. Wu, J. Chang, A review of bioactive silicate ceramics, Biomed. Mater. 8 (3) (2013), https://doi.org/10.1088/1748-6041/8/3/032001, 032001, abr.

[17] L. Wu, F. Feyerabend, A.F. Schilling, R. Willumeit-Römer, B.J.C. Luthringer, Effects of extracellular magnesium extract on the proliferation and differentiation of human osteoblasts and osteoclasts in coculture, Acta Biomater. 27 (2015) 294–304, https://doi.org/10.1016/j.actbio.2015.08.042, nov.

[18] D. Hu, et al., Different response of osteoblastic cells to Mg^{2+}, Zn^{2+} and Sr^{2+} doped calcium silicate coatings, J. Mater. Sci. Mater. Med. 27 (3) (2016) 56, https://doi.org/10.1007/s10856-016-5672-y, mar.

[19] C. Wu, J. Chang, Degradation, bioactivity, and cytocompatibility of diopside, akermanite, and bredigite ceramics, J. Biomed. Mater. Res. B Appl. Biomater. 83B (1) (2007) 153–160, https://doi.org/10.1002/jbm.b.30779, oct.

[20] S. Castiglioni, A. Cazzaniga, W. Albisetti, J. Maier, Magnesium and osteoporosis: current state of knowledge and future research directions, Nutrients 5 (8) (2013) 3022–3033, https://doi.org/10.3390/nu5083022, jul.

[21] M. Diba, O.-M. Goudouri, F. Tapia, A.R. Boccaccini, Magnesium-containing bioactive polycrystalline silicate-based ceramics and glass-ceramics for biomedical applications, Curr. Opin. Solid State Mater. Sci. 18 (3) (2014) 147–167, https://doi.org/10.1016/j.cossms.2014.02.004, jun.

[22] E. Fiume, G. Serino, C. Bignardi, E. Verné, F. Baino, Bread-derived bioactive porous scaffolds: an innovative and sustainable approach to bone tissue engineering, Molecules 24 (16) (2019) 2954, https://doi.org/10.3390/molecules24162954, aug.

[23] M.A. Sainz, P. Pena, S. Serena, A. Caballero, Influence of design on bioactivity of novel $CaSiO_3$–$CaMg(SiO_3)_2$ bioceramics: in vitro simulated body fluid test and thermodynamic simulation, Acta Biomater. 6 (7) (2010) 2797–2807, https://doi.org/10.1016/j.actbio.2010.01.003, jul.

[24] J.S. Cho, Y.C. Kang, Synthesis of spherical shape borate-based bioactive glass powders prepared by ultrasonic spray pyrolysis, Ceram. Int. 35 (6) (2009) 2103–2109, https://doi.org/10.1016/j.ceramint.2008.11.010, aug.

[25] S. Hayashi, K. Okada, N. Otsuka, T. Yano, Preparation and characterization of diopside powder by several methods from solution, J. Mater. Sci. Lett. 12 (3) (1993) 153–156, https://doi.org/10.1007/BF00819943.

[26] N.Y. Iwata, G.-H. Lee, Y. Tokuoka, N. Kawashima, Sintering behavior and apatite formation of diopside prepared by coprecipitation process, Colloids Surf. B Biointerfaces 34 (4) (2004) 239–245, https://doi.org/10.1016/j.colsurfb.2004.01.007, abr.

[27] P. Saravanapavan, J.R. Jones, R.S. Pryce, L.L. Hench, Bioactivity of gel-glass powders in the CaO-SiO_2 system: a comparison with ternary (CaO-P_2P_5-SiO_2) and quaternary glasses (SiO_2-CaO-P_2O_5-Na_2O), J. Biomed. Mater. Res. 66A (1) (2003) 110–119, https://doi.org/10.1002/jbm.a.10532, jul.

[28] D. Arcos, M. Vallet-Regí, Sol–gel silica-based biomaterials and bone tissue regeneration, Acta Biomater. 6 (8) (2010) 2874–2888, https://doi.org/10.1016/j.actbio.2010.02.012, aug.

[29] P. Sepulveda, J.R. Jones, L.L. Hench, Characterization of melt-derived 45S5 and sol-gel-derived 58S bioactive glasses, J. Biomed. Mater. Res. 58 (6) (2001) 734–740, https://doi.org/10.1002/jbm.10026.

[30] R. Ciriminna, A. Fidalgo, V. Pandarus, F. Béland, L.M. Ilharco, M. Pagliaro, The sol–gel route to advanced silica-based materials and recent applications, Chem. Rev. 113 (8) (2013) 6592–6620, https://doi.org/10.1021/cr300399c, aug.

[31] S.N.L. Ramlee, N.S.A.N. Sharifulden, H. Mohamad, S.N.F.M. Noor, Sol-gel derived bioactive glass scaffolds incorporated with polyvinyl-alcohol and pluronic P123 polymers using sponge replication technique, Mater. Today Proc. 17 (2019) 966–975, https://doi.org/10.1016/j.matpr.2019.06.463.

[32] C. Yamagata, J.B. Andrade, V. Ussui, N.B. de Lima, J.O.A. Paschoal, High purity zirconia and silica powders via wet process: alkali fusion of zircon sand, Mater. Sci. Forum 591–593 (2008) 771–776, aug, https://doi.org/10.4028/www.scientific.net/MSF.591-593.771.

[33] R. Choudhary, S. Koppala, S. Swamiappan, Bioactivity studies of calcium magnesium silicate prepared from eggshell waste by sol–gel combustion synthesis, J. Asian Ceram. Soc. 3 (2) (2015) 173–177, https://doi.org/10.1016/j.jascer.2015.01.002, jun.
[34] T. Kokubo, H. Takadama, How useful is SBF in predicting in vivo bone bioactivity? Biomaterials 27 (15) (2006) 2907–2915, https://doi.org/10.1016/j.biomaterials.2006.01.017, may.
[35] F. Baino, S. Hamzehlou, S. Kargozar, Bioactive glasses: where are we and where are we going? J. Funct. Biomater. 9 (1) (2018) 25, https://doi.org/10.3390/jfb9010025, mar.
[36] L.L. Hench, R.J. Splinter, W.C. Allen, T.K. Greenlee, Bonding mechanisms at the interface of ceramic prosthetic materials, J. Biomed. Mater. Res. 5 (6) (1971) 117–141, https://doi.org/10.1002/jbm.820050611, nov.
[37] E. El-Meliegy, R. van Noort, Glasses and Glass Ceramics for Medical Applications, Springer, New York, NY, 2012, https://doi.org/10.1007/978-1-4614-1228-1. New York.
[38] Principles of designing glass-ceramic formation, in: Glass-Ceramic Technology, John Wiley & Sons, Inc., Hoboken, NJ, USA, 2012, pp. 1–74, https://doi.org/10.1002/9781118265987.ch1.
[39] R.D. Rawlings, J.P. Wu, A.R. Boccaccini, Glass-ceramics: their production from wastes—a review, J. Mater. Sci. 41 (3) (2006) 733–761, https://doi.org/10.1007/s10853-006-6554-3, feb.
[40] ISO 10993-5, Biological Evaluation of Medical Devices — Part 5: Tests for In-Vitro Cytotoxicity, 2009.
[41] M. Mozafari, S. Banijamali, F. Baino, S. Kargozar, R.G. Hill, Calcium carbonate: adored and ignored in bioactivity assessment, Acta Biomater. 91 (2019) 35–47, https://doi.org/10.1016/j.actbio.2019.04.039, jun.
[42] G.E.A. Swann, S.V. Patwardhan, Application of Fourier Transform Infrared Spectroscopy (FTIR) for assessing biogenic silica sample purity in geochemical analyses and palaeoenvironmental research, Clim. Past 7 (1) (2011) 65–74, https://doi.org/10.5194/cp-7-65-2011, feb.
[43] A.S. Khan, et al., Vibrational spectroscopy of selective dental restorative materials, Appl. Spectrosc. Rev. 52 (6) (2017) 507–540, https://doi.org/10.1080/05704928.2016.1244069, jul.
[44] H. Gheisari, E. Karamian, M. Abdellahi, A novel hydroxyapatite –Hardystonite nanocomposite ceramic, Ceram. Int. 41 (4) (2015) 5967–5975, https://doi.org/10.1016/j.ceramint.2015.01.033, may.
[45] A. Ślósarczyk, Z. Paszkiewicz, C. Paluszkiewicz, FTIR and XRD evaluation of carbonated hydroxyapatite powders synthesized by wet methods, J. Mol. Struct. 744 (747) (2005) 657–661, https://doi.org/10.1016/j.molstruc.2004.11.078, jun.